Stem Cell Reports
Article

ISSCR

OPEN ACCESS

3D In Vitro Model of a Functional Epidermal Permeability Barrier from Human Embryonic Stem Cells and Induced Pluripotent Stem Cells

Anastasia Petrova,[1,2,9] Anna Celli,[3] Laureen Jacquet,[1] Dimitra Dafou,[4,10] Debra Crumrine,[3] Melanie Hupe,[3] Matthew Arno,[5] Carl Hobbs,[6] Aleksandra Cvoro,[7] Panagiotis Karagiannis,[2] Liani Devito,[1] Richard Sun,[3] Lillian C. Adame,[3] Robert Vaughan,[8] John A. McGrath,[2] Theodora M. Mauro,[3,*] and Dusko Ilic[1,*]

[1]Stem Cell Laboratory, Assisted Conception Unit, Division of Women's Health, Women's Health Academic Centre, King's College London, London SE1 9RT, UK
[2]St John's Institute of Dermatology, King's College London, London SE1 9RT, UK
[3]Department of Dermatology, Veteran Affairs Medical Center, University of California, San Francisco, San Francisco, CA 94121, USA
[4]Division of Genetics and Molecular Medicine, King's College London School of Medicine, Guy's Hospital, London SE1 9RT, UK
[5]Genomics Centre, King's College London, London SE1 9NH, UK
[6]Histology Laboratory, Wolfson Centre for Age-Related Diseases, School of Biomedical Sciences, King's College London, London SE1 1UL, UK
[7]Genomic Medicine, The Methodist Hospital Research Institute, Houston, TX 77030, USA
[8]Clinical Transplantation Laboratory, GSTS and MRC Centre for Transplantation, King's College London, King's Health Partners, London SE1 9RT, UK
[9]Present address: Immunobiology Unit, Institute of Child Health, University College London, London WC1N 1EH, UK
[10]Present address: School of Biology, Department of Genetics, Development and Molecular Biology, Aristotle University, 54124 Thessaloniki, Greece
*Correspondence: maurot@derm.ucsf.edu (T.M.M.), dusko.ilic@kcl.ac.uk (D.I.)
http://dx.doi.org/10.1016/j.stemcr.2014.03.009

SUMMARY

Cornification and epidermal barrier defects are associated with a number of clinically diverse skin disorders. However, a suitable in vitro model for studying normal barrier function and barrier defects is still lacking. Here, we demonstrate the generation of human epidermal equivalents (HEEs) from human embryonic stem cells (hESCs) and induced pluripotent stem cells (iPSCs). HEEs are structurally similar to native epidermis, with a functional permeability barrier. We exposed a pure population of hESC/iPSC-derived keratinocytes, whose transcriptome corresponds to the gene signature of normal primary human keratinocytes (NHKs), to a sequential high-to-low humidity environment in an air/liquid interface culture. The resulting HEEs had all of the cellular strata of the human epidermis, with skin barrier properties similar to those of normal skin. Such HEEs generated from disease-specific iPSCs will be an invaluable tool not only for dissecting molecular mechanisms that lead to epidermal barrier defects but also for drug development and screening.

INTRODUCTION

The major function of the skin is to form a permeability barrier between an organism and its external environment. Integrity and cohesion of the "bricks and mortar" structure of the outermost layer of epidermis, the stratum corneum (SC), is essential for terrestrial life, the survival of which ultimately depends on maintenance of permeability barrier homeostasis (Elias, 1983; Kalinin et al., 2002; Segre 2003). The SC is composed of corneocytes ("bricks") encased in a lipid-rich extracellular matrix (ECM; "mortar") (Nemes and Steinert, 1999).

Corneocytes, which are composed of keratin microfibrils surrounded by cornified envelopes (CEs), are the final products of a linear keratinocyte differentiation pathway from a mitotically active stratum basale (SB) through a transcriptionally active stratum spinosum (SS) and a stratum granulosum (SG) that transitions into anucleate SC cells. The CEs are formed from precursor proteins directly beneath the plasma membrane. Following membrane disintegration, Ca^{2+} influx activates transglutaminase, which irreversibly crosslinks CE proteins around filaggrin-associated keratin filaments. These CEs combine with secreted and processed lipids to form a functional epidermal barrier.

The lipids are packaged into lamellar bodies in the SG cells. The lamellar body, with all its contents, is secreted in response to barrier perturbation. The secreted lipids of the SC are processed into lamellar membranes (Figures 1A and 1B). Lamellar bodies also contain proteolytic enzymes and antimicrobial peptides, which when secreted along with lipid contribute to permeability barrier function (reviewed in Elias, 2012).

Ichthyoses and atopic dermatitis are due to polymorphisms or mutations in genes that control keratinocyte differentiation, cornification, or lipid metabolism. These changes lead to defects in epidermal permeability barrier homeostasis that range from mild (can be easily mistaken for normal dry skin) to life threatening (Segre 2006; Smith et al., 2006; Richard, 2004). Although ichthyosis-like diseases are also present in animals and can be mimicked in transgenic mouse models, there are still no suitable in vitro models for these diseases.

Human epidermal equivalents (HEEs) are in-vitro-generated 3D models that are widely used in experimental settings. However, their utility for addressing the mechanisms

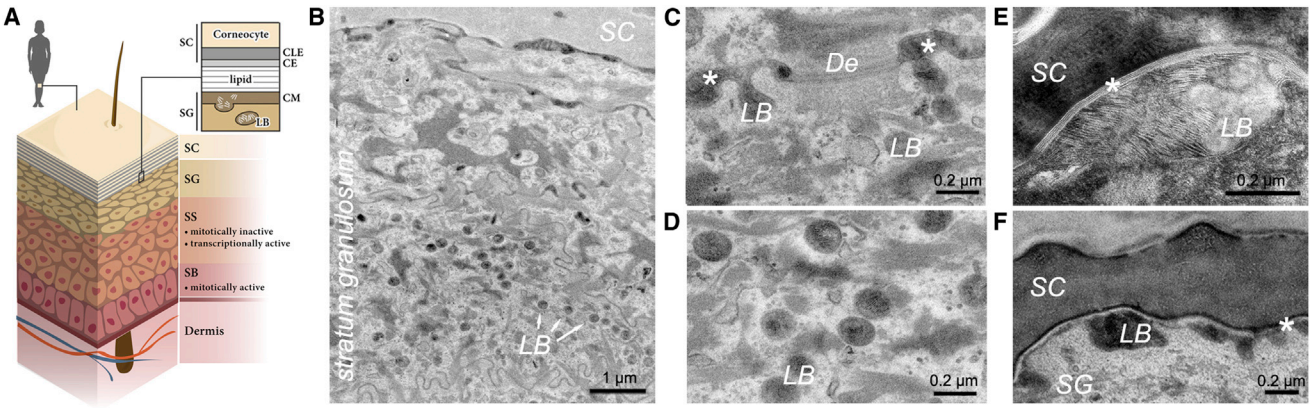

Figure 1. Epidermal Permeability Barrier within the SC of Normal Human Skin

(A) Schematic drawing of normal human skin, depicting the epidermal permeability barrier within the SC.

(B–F) TEM demonstrates the components of a competent permeability barrier in normal human skin. Lipids are packaged into lamellar bodies (LBs) in the SG cells.

(B) LBs (arrows) are present in the uppermost SG cells. These LBs are not discrete droplets, but rather are part of a tubular network extending from the Golgi.

(C) LBs, with all their contents, are secreted into extracellular space (asterisks) between the uppermost SG cells. De, desmosome.

(D) Close-up of LB morphology.

(E) Lipid from LBs is processed into lipid bilayers (asterisk) by SC enzymes that require acidity, thus forming lipid structures that are impermeable to passage of water and ions.

(F) Ceramide-based lipids bind to the CE (asterisk), forming the cornified lipid envelope (CLE).

Scale bars are noted in each panel.

of various skin disorders, or for drug development and testing, has been limited by the fact that previously engineered HEEs do not form a fully developed epidermal barrier. In spite of advances in HEE engineering, such as integrating melanocytes (Nissan et al., 2011), macrophages (Linde et al., 2012), or dermal fibroblasts (Itoh et al., 2013) and pluristratified epidermis, issues involving the generation of a functional permeability barrier in vitro remain unresolved. Further, in vitro studies have been limited by the fact that only a limited number of HEEs can be generated from one sample of epidermis, and the primary keratinocytes generated from this sample may contain previously unidentified polymorphisms in genes that modify epidermal growth, differentiation, or barrier development. HEEs generated from immortalized keratinocytes develop even less well than those generated from primary keratinocytes (Götz et al., 2012). Therefore, in order to develop a HEE model that can be produced in an unlimited number of genetically identical units, we turned to human embryonic stem cells (hESCs) and induced pluripotent stem cells (iPSCs), primary cells that are capable of infinite proliferation and whose genetic footprint can be fully characterized.

We demonstrate here that by following an integrated, highly reproducible four-step protocol, we were able to differentiate hESCs/iPSCs into keratinocytes with gene-expression profiles similar to those of normal human keratinocytes (NHKs, i.e., primary keratinocytes isolated from biopsies of normal healthy skin). These hESC/iPSC-derived keratinocytes were then used to generate HEEs in an air/liquid interface culture exposed to sequential a high-to-low humidity environment. HEEs generated from hESC/iPSC-derived keratinocytes have a functional permeability barrier similar to native human skin and are indistinguishable from HEEs generated from NHKs under the same condition. We are not aware of any other protocols resulting in this functional endpoint.

RESULTS

Reprogramming

Since the first iPSCs were derived, different reprogramming approaches aimed at increasing their efficiency and minimizing the potential for DNA damage have been developed (reviewed in Bellin et al., 2012; Robinton and Daley 2012). We used a nonintegrating, nonviral, synthetic, modified mRNA system (Yakubov et al., 2010; Warren et al., 2010) to reprogram human newborn fibroblasts (Figure S1 available online). In our hands, the reprogramming efficiency was ~0.76% (Figures 2A and S2), which is lower than that reported by Warren et al. (2010). We chose two iPSC clones, iKCL004 and iKCL011, that had a population doubling time (PDT) similar to that of KCL034, a clinical-grade

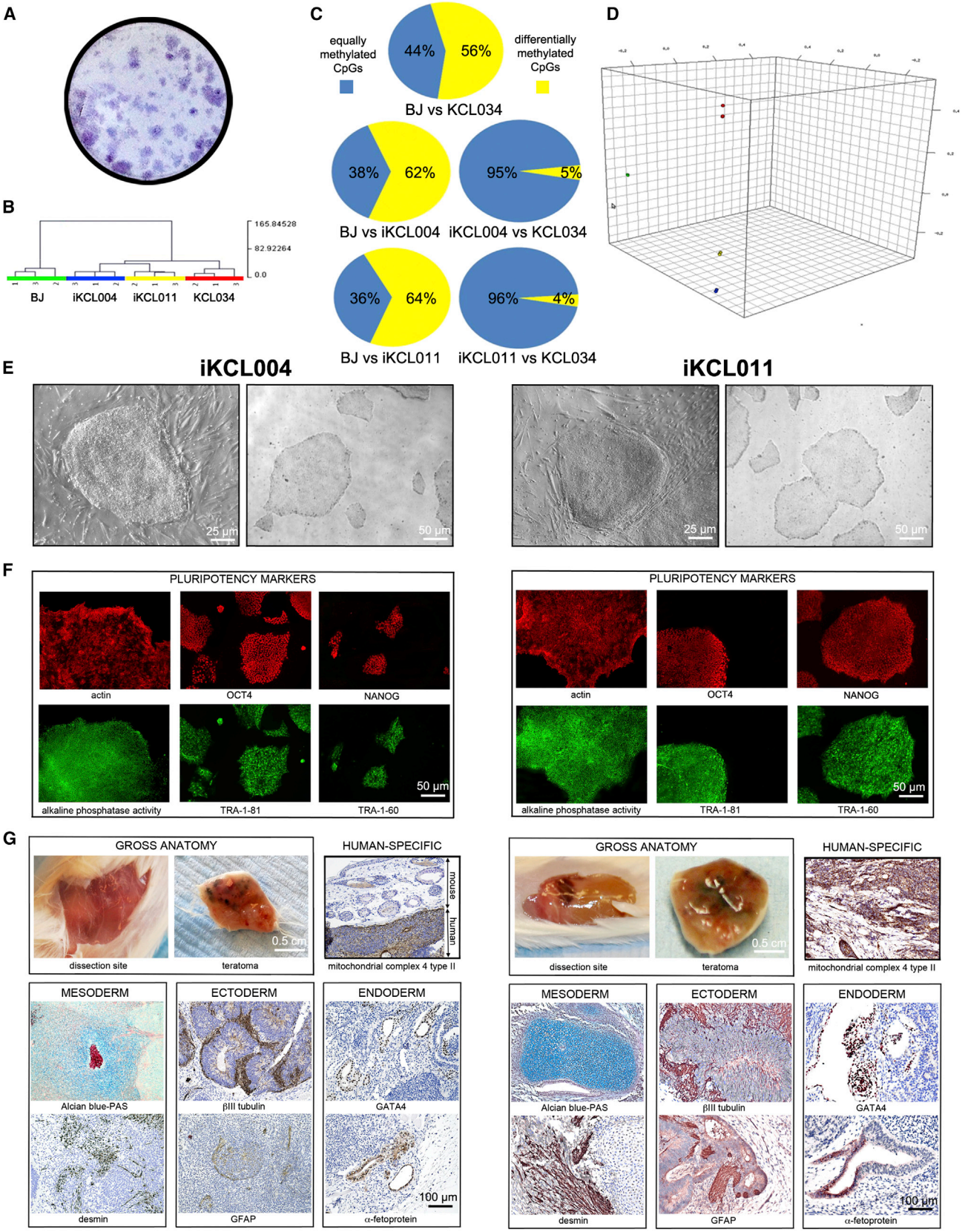

(legend on next page)

hESC line that we used as a control throughout all experiments. Both iKCL004 and iKCL011 had a methylation signature of PSCs, expressed pluripotency markers, and were able to differentiate into cells of all three germ layers in vivo (Figures 2B–2G and S3). Array comparative genomic hybridization (CGH) did not detect any copy number changes, using Promega male as a standard, over an extended period of cell culture (>3 months) under feeder-free conditions.

Efficient and Reproducible Differentiation of hESCs and iPSCs into Keratinocytes

To recapitulate epidermogenesis, in the first step of keratinocyte differentiation, which we termed "induction," we transferred a clinical-grade hESC line (KCL034) and two iPSC lines (iKCL004 and iKCL011) from 5% O_2 to atmospheric O_2, and exposed them to 25 ng/ml BMP4 and 1 μM of the carboxylic acid form of vitamin A, all-*trans* retinoic acid (ATRA), for 7 days (Figure 3A). The lines did not respond similarly to induction. Both iPSC lines expressed higher mRNA levels of the epidermal markers integrin β4 (*ITGB4*) and keratin 14 (*KRT14*), suggesting differentiation toward an epidermal lineage, whereas hESC line KCL034 seemed to remain "undecided," having similar mRNA levels of these two epidermal markers and a neural marker, oligodendrocyte lineage transcription factor 2 (*OLIG2*; Figure 3B). In the next step, termed "selection," we used native 3D decellularized human dermal fibroblast (HDF) ECM as a growth-supporting platform. This was done to mimic basement membrane (BM), which is formed soon after epidermal induction during embryogenesis (Figure S4). A week later, we purified epidermal progenitor stem cells based on their preferential adherence to collagen IV (Murray et al., 1979; Bickenbach and Roop, 1999). During the next "enrichment" step of our differentiation protocol, the purified cells gave rise to a homogeneous population of keratin 14 $(K14)^+p63^+$ colonies, which was further amplified in the final "expansion" step of the protocol (Figure 3C). p63 is a transcription factor that plays a major role in maintaining the proliferative potential of epithelial progenitors (reviewed in Blanpain and Fuchs, 2007). Whereas plating of cells on 3D HDF ECM rapidly increased *p63* mRNA expression, pluripotent markers, such as the transcription factors *Oct4* and *nanog*, steadily decreased during differentiation (Figure 3D). K18, which is expressed earliest during embryonic development, and with its binding partner K8 can serve as a marker of simple epithelium, was expressed at higher levels only during the induction and selection steps, suggesting that the cells subjected to our differentiation protocol were following a fate similar to that which occurs for epidermal morphogenesis during embryonic development. This four-step protocol was highly reproducible. *KRT14* expression increased steadily during differentiation and there were no significant differences among the three lines in multiple rounds of the differentiation process (Figure 3E). The PD of hESC/IPSC-derived keratinocytes did not differ much from that of NHKs over a period of 5 weeks in culture (Figure 3F).

hESC/iPSC-Derived Keratinocytes Are Very Similar to Primary NHKs

Next, we compared enriched and expanded populations (T3) of hESC/iPSC-derived keratinocytes with NHKs from different donors in several different ways, and did not find any major discrepancies. Differences in the expression levels of *KRT14* and *p63* in multiple T3 populations of hESC/iPSC-derived keratinocytes (n = 9; three biological repeats for each of three lines) and NHKs from three donors were not statistically significant (Figure 4A). Flow-cytometry analysis of NHK and T3 populations of hESC/iPSC-derived keratinocytes using K14 and integrin β4 as markers did not identify any marked difference in the percentage of double-positive (DP) cells; 95% of NHK, 87.8% of

Figure 2. Generation and Characterization of Normal Human iPSCs

(A) Trypan blue staining of colonies in one well of a six-well dish. The average reprogramming efficiency from two independent experiments was ~0.76%.

(B–D) DNA methylation analyses. Hierarchical clustering (B), methylation portrait (C), and principal component analysis (D) suggest that both iKCL004 and iKCL011 have the methylation signature of PSCs. BJ, parental HFFs. n = 3 biological replicates (rounds of differentiation) for each cell line.

(D) Undifferentiated iKCL004 and iKCL011 cultured on HFF feeders and under feeder-free conditions display the typical morphology of PSCs.

(E) Expression of pluripotency markers is confirmed by alkaline phosphatase (AP) activity assay and immunostaining for NANOG, OCT4, TRA-160, and TRA-1-81 in iKCL004 and iKCL011 lines.

(F) Differentiation of iKCL004 and iKCL011 into all three germ layers in vivo is confirmed by detection of specific markers. Teratomas were encapsulated and did not invade surrounding tissues. All sections were stained with hematoxylin and eosin (H&E). Specific stains are brown (immunohistochemistry) or light blue (Alcian). Positive staining for mitochondrial complex IV type II confirms the human origin of the teratoma tissue. Germ layer markers: Alcian blue/periodic acid Schiff (PAS)-stained cartilage and desmin for mesoderm, βIII tubulin and glial fibrillary acidic protein (GFAP) for ectoderm, and GATA4 and α-fetoprotein for endoderm.

See also Figures S1–S3.

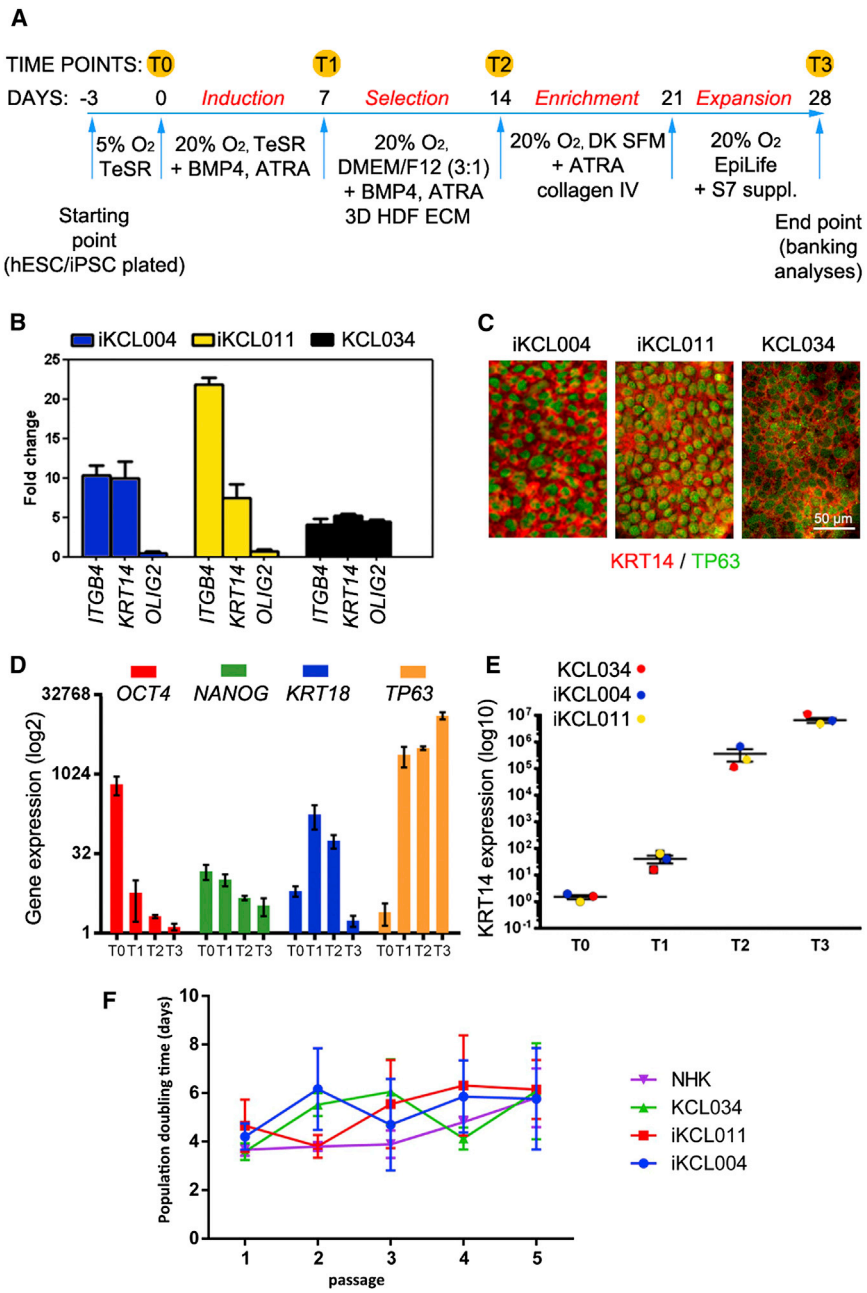

Figure 3. Efficient and Reproducible Differentiation of hESCs and iPSCs into Keratinocytes

(A) Schematic of the differentiation protocol. T0 (day 0), T1 (day 7), T2 (day 14), and T3 (day 28) represent time points at which the cells were switched to a new culture condition and/or collected for analyses.

(B) qPCR analysis measuring the expression of differentiation markers (epidermal: *ITGB4* and *KRT14*; neural: *OLIG2*) suggests a difference in commitment toward epidermal lineage at time point T1. n = 9 for each cell line; each of three rounds of differentiations (biological replicates) had three technical replicates.

(C) Diversity is lost at later stages, and cell colonies at the enrichment step are uniformly positive for keratinocyte markers K14 (red) and p63 (green).

(D) qPCR analyses measuring expression of differentiation markers at T0, T1, T2, and T3 of the differentiation protocol. Expression of pluripotency markers *OCT4* and *NANOG* is diminished by the end of differentiation, whereas *KRT18* and *p63* mRNA levels reflect stages during epidermogenesis. n = 9 for each cell line; each of three rounds of differentiations (biological replicates) had three technical replicates.

(E) Levels of *KRT14* mRNA expressed during three rounds of differentiation at four different time points for each of lines demonstrate the reproducibility of the protocol. Absolute quantification was performed using the ddCt method. GOI expression was normalized to the geometrical mean of two HK genes (*GAPDH* and *EIF4A2*). The SEM was calculated for mean expression in KCL034, iKCL004, and iKCL011. n = 9 for each cell line; each of three biological replicates/rounds of differentiations had three technical replicates.

(F) The proliferation rate of hESC/iPSC-derived keratinocytes shows no marked difference compared with freshly isolated primary NHKs over a period of 5 weeks. Statistical significance was calculated for each passage using two-way ANOVA with Sidak's multiple comparison test. Data are presented as a blank adjusted mean with SD (n = 3 biological replicates for each cell line).

See also Figure S4.

KCL034 T3, 95.4% of iKCL004 T3, and 86% of iKCL011 T3 were K14$^+$/integrin β4$^+$ (Figures 4B and S5). Finally, we used the HumanHT-12 Expression BeadChip whole-genome expression array, which provides coverage for more than 47,000 transcripts and known splice variants, to compare the transcriptomes of undifferentiated hESCs/iPSCs (T0), hESC/iPSC-derived keratinocytes (T3), and NHKs from two different donors. The T0 and T3 transcriptomes were analyzed as biological replicates from three independent differentiation runs for each of three cell lines (KCL034, iKCL004, and iKCL011). Principal component analysis identified an expected pattern: hESC/iPSC-derived keratinocytes at T3 were grouped together with NHKs and were dissimilar to undifferentiated hESCs/iPSCs at T0

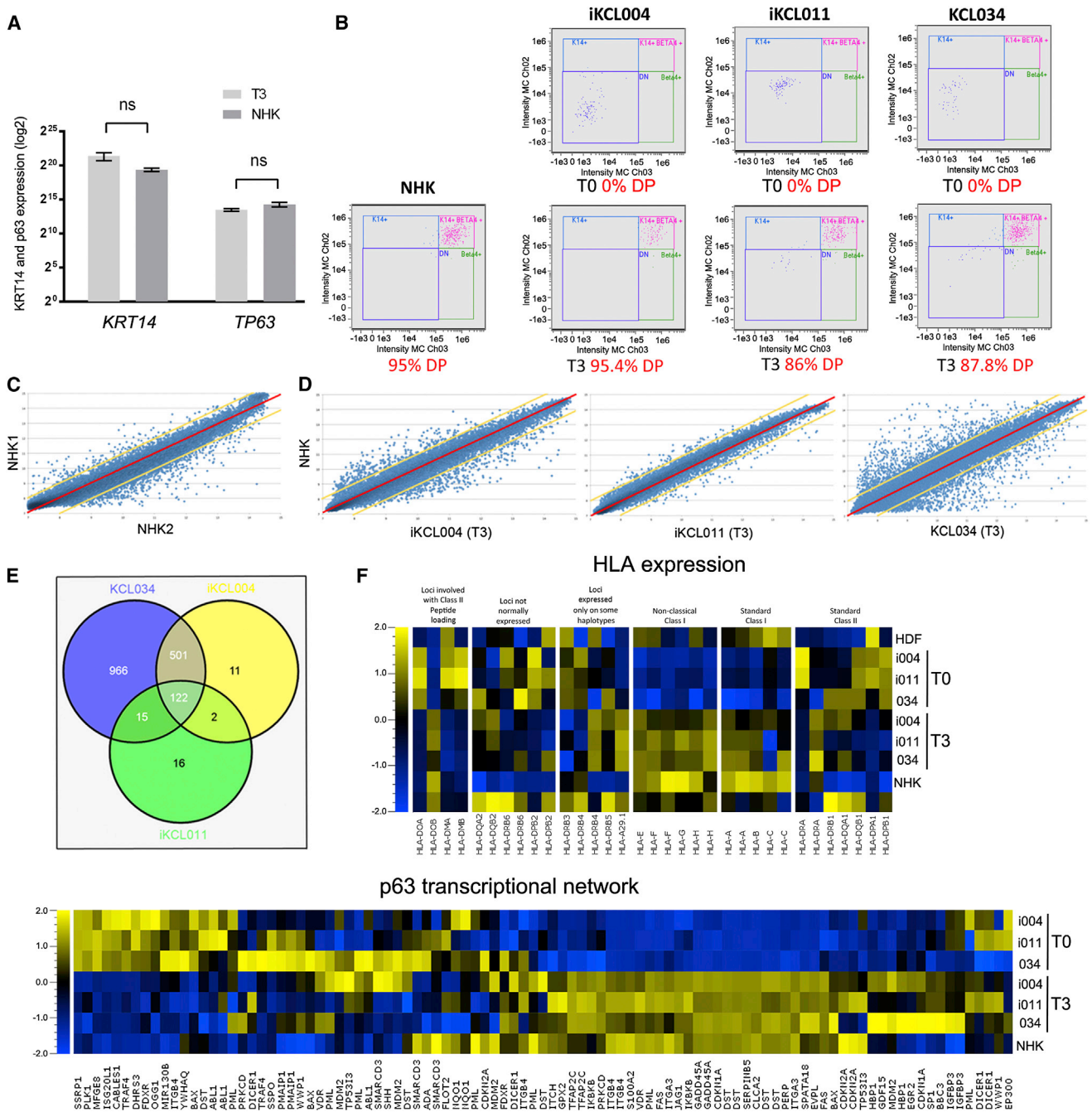

Figure 4. Profiling of hESC/iPSC-Derived Keratinocytes

(A) qPCR analyses measuring expression of *KRT14* and *p63* in hESC/iPSC-derived keratinocytes at T3 (n = 9; three rounds of differentiation for each of three lines) and NHKs (n = 2) found no significant difference between the two groups. Multiple t tests. Statistical significance was determined using the Holm-Sidak method. For *KRT14*, p = 0.120881; for *p63*, p = 0.155472.

(B) Populations of hESC/iPSC-derived keratinocytes at T3 have a similar percentage of $K14^+$/integrin $\beta4^+$ cells as NHKs. The percentage is an average from three rounds of differentiation for each of the three lines. At T0, no $K14^+$/integrin $\beta4^+$ cells were detected. Fluorescence-activated cell sorting (FACS) images represent one of the three rounds.

(C and D) Scatterplots showing the relative expression of all genes on the chip.

(C) Global gene-expression profiles of NHKs from two donors (NHK1 and NHK2) shown as a scatterplot against each other.

(legend continued on next page)

(Figure S6). As an average of three biological replicates, the transcriptome of iKCL011-derived keratinocytes at T3 was closer to the transcriptome of NHKs than to keratinocytes derived from iKCL004 or KCL034. A scatter analysis of gene expression in NHKs from two different donors (NHK1 and NHK2) found that 939 transcripts (2.00%) differed by >2-fold (Figure 4C). An average of these two was then compared with an average of three biological replicates from each of the three lines at T3. The keratinocytes derived from iKCL011 differed by >2-fold in only 155 transcripts (0.33%) from NHKs by >2-fold, whereas iKCL004 (636 transcripts, 1.35%) and KCL034 (1,604 transcripts, 3.41%) were more distinct (Figure 4D). Among all transcripts that were different from NHKs, only 122 (0.26%) were common to all hESC/iPSC-derived keratinocytes at T3 (Figure 4E). We profiled these 122 transcripts using the GeneGo database (Thomson Reuters) for Pathway Maps, Process Networks, Gene Ontology Networks, and Disease Biomarkers list, and found that 34 (0.07%) of them might have relevance to keratinocyte biology (Tables S1–S5, S6, and S7).

We also looked at how reprogramming and differentiation changed human leukocyte antigen (HLA) gene expression (Figure 4F). Although parental HDFs do express HLA class I, the reprogrammed clonal lines iKCL004 and iKCL011 do not, similarly to hESC line KCL034. Differentiation into keratinocytes changed the global pattern. Notably, HLA class I genes were turned on, implying that the recipients of epidermis generated from the hESC-derived keratinocytes as an off-shelf product would be in need of immunosuppressive therapy, whereas that may not be the case with iPSC-based autografts.

hESC-derived keratinocytes exhibit an epidermal transcription program, and p63 is considered to be the main transcription regulator of epidermogenesis and essential for epidermal commitment of hESCs (Blanpain and Fuchs, 2007; Aberdam et al., 2007; Medawar et al., 2008; Pozzi et al., 2009; Crum and McKeon 2010; Vanbokhoven et al., 2011). Therefore, we compared the expression profiles of 96 genes that, according to the NCI Pathway Interaction Database, constitute the p63 transcriptional network. Of these genes, only three (*ADA* [OMIM: 608958], *SMARCD3* [OMIM: 601737], and *YWHAQ* [OMIM: 609009] had ≥2-fold higher expression in NHK from two donors than in all biological replicates of hESC/iPSC-derived keratinocytes at T3. Similarly, only three of those 96 genes (*BBC3* or *PUMA* [OMIM: 605854], *CDKN1A* or *p21* [OMIM: 116899], and *SP1* [OMIM: 189906]) had ≥2-fold higher expression in hESC/iPSC-derived keratinocytes at T3 than in NHKs from two donors. None of these six genes are known to be essential for epidermogenesis, although they may be indirectly involved.

HEEs with a Functional Epidermal Permeability Barrier Generated In Vitro

Molecular characterization suggested that our highly reproducible protocol for differentiating hESCs/iPSCs into keratinocytes yields a fairly pure population of cells that are very similar to NHK. To test the capability of hESC/iPSC-derived keratinocytes to generate multilayered epithelium in vitro, we used the HEE model developed by R.S., A.C., D.C., M.H., L.C., S.D. Peckenpacker, K. Park, Y. Uchida, K.R. Feingold, P.M. Elias, D.I., and T.M.M. (unpublished data). The HEEs generated using this protocol developed in vitro all of the cellular strata seen in the human epidermis. Since they also developed normal barrier properties in vitro, there was no need to implant the organotypic cultures into immunodeficient mice, which is a commonly used technique (Del Rio et al., 2002). We assessed the integrity of the stratifying cultures by measuring the transepithelial electric resistance (TEER), which indicates changes in the transcellular and paracellular permeability of epithelial/epidermal in vitro cell cultures. Within 2 weeks, the TEER in all cultures reached >1,000 Ω, indicating the formation of a permeability barrier and multilayered epithelia (Figures 5A and 5B).

Differentiation markers were normally expressed and located (Figures 6A–6D). Since our system does not contain mixed fibroblast-keratinocytes cultures, the basement membrane zone (BMZ) generated by this system cannot

(D) Global gene-expression profiles of hESC/iPSC-derived keratinocytes at T3 (average of n = 3 biological replicates/rounds of differentiation for each line) shown in scatterplots against NHKs (average of n = 2). Normalized linear expression levels for each probe are plotted as XY coordinates for each sample. Yellow lines indicate boundaries of a 2-fold relative expression difference.
(E) Venn diagram of the transcripts with a 2-fold relative expression difference from NHKs in KCL034-, iKCL004-, and iKCL011-derived keratinocytes at T3 shows that 122 out of >47,000 were common to all three lines.
(F) Heatmaps showing relative expression patterns across multiple samples for specific gene lists. HLA genes were selected by text searching for "HLA" within the "Gene Symbol" annotation, and p63-related genes were identified from the p63 transcriptional network in the NCI Pathway Interaction database. The colors of the heatmaps indicate high (yellow) or low (blue) expression relative to the average for that gene across the samples. The values are the average of three independent runs for KCL034, iKCL004, and iKCL011 at T0 and T3. Transcripts for NHKs from two different donors are shown independently on the HLA heatmap, and as an average on the p63 transcriptional network heatmap.
See also Figures S5 and S6, and Tables S1–S5, S6, and S7.

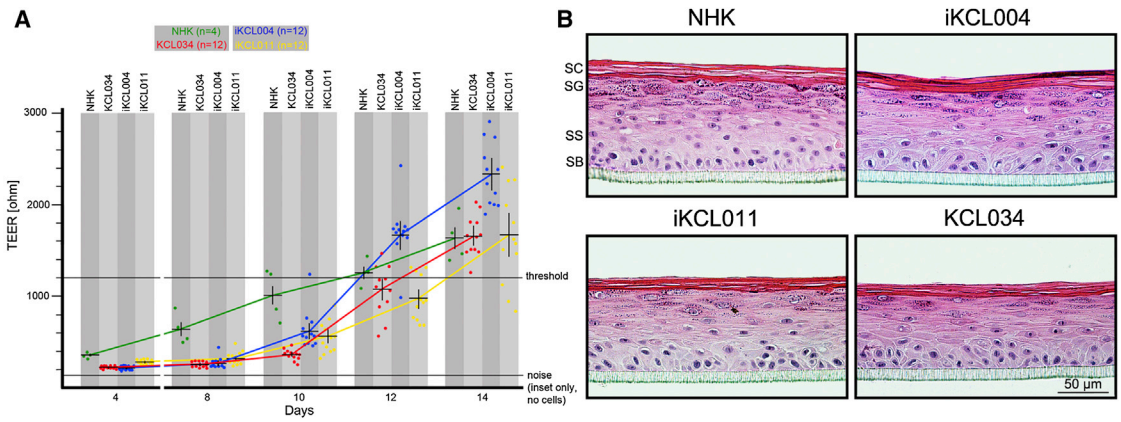

Figure 5. Pluristratified HEEs Generated In Vitro from hESCs and iPSCs

(A) The TEER during HEE formation over a period of 14 days reflects permeability barrier formation (n = 4 for NHK, n = 12 for each of lines; each point represents an average of measurements from three different spots). Error bars represent SD. Only 14-day-old HEE cultures that displayed a TEER of >1,200 ohm cm^2 were used for subsequent analyses unless indicated otherwise.

(B) H&E staining demonstrates normal morphology with the presence of all epidermal layers regardless of the source of keratinocyte population. SB, stratum basale; SS, stratum spinosum.

be equivalent to the BMZ of human skin. Nevertheless, in our 3D cultures, basal-layer keratinocytes were secreting ECM proteins, such as laminin, and assembling a BMZ-like structure (Figures 6E and 6F).

Next, we examined the epidermal permeability barrier. Lipid secretion appeared normal. Lamellar bodies and extensive intercellular bilayers were detected in all cultures (Figure 7A). The endoplasmatic reticulum (ER) Ca^{2+} store, which is essential for normal keratinocyte signaling and differentiation (Callewaert et al., 2003; Celli et al., 2012), was detectable at day 8 of the culture (Figure 7B). Typically, the Ca^{2+} gradient for normal epidermis has low levels in the SB and lowest levels in the SS, followed by an increase in extra- and intracellular Ca^{2+} that peaks within the SG (Elias et al., 2002). In terminally differentiated air-lifted cultures at day 14, HEEs generated from NHKs and hESC (KCL034)-derived keratinocytes had the greatest density of Ca^{2+} precipitates in the SG, whereas precipitates were somewhat more diffuse in HEEs generated from iPSC-derived keratinocytes (Figure 7C). However, the lanthanum perfusion assay, which is used to depict pathways of water movement through epidermis, demonstrated a functional permeability barrier in all cultures: the passage of electron-dense lanthanum tracer was blocked by the epidermal lipid barrier at the SG/SC interface and was not detected in the SC (Figure 7D).

DISCUSSION

We have described a stepwise protocol for manufacturing in vitro HEEs, with all of the cellular strata and apparently normal barrier properties seen in the human epidermis, from hESCs and iPSCs.

When manipulating the cellular fate of pluripotent cells in vitro, it is crucial to have a thorough understanding of the embryonic morphogenesis of the target tissue in order to achieve efficient production of the desired cell type (Hay et al., 2008; Cheng et al., 2012). Epidermal morphogenesis and homeostasis are relatively well described (Blanpain and Fuchs, 2009; Simpson et al., 2011). After gastrulation, the embryo surface emerges as a single layer of neuroectoderm, which will ultimately specify the nervous system and skin epithelium. This decision is guided by Wnt signaling, which blocks the ability of the ectoderm to respond to fibroblast growth factors (FGFs). In the absence of FGF signaling, the cells express bone morphogenetic proteins (BMPs) and become fated to develop into epidermis. In contrast, neural fate develops when, in the absence of a Wnt signal, the ectoderm is able to receive and translate activating cues by FGFs, which then attenuate BMP signaling through inhibitory cues (Chang and Hemmati-Brivanlou, 1998; Stern, 2005). Similarly to our protocol, most of the published protocols for differentiation of PSCs (either mouse or human) into keratinocytes follow this strategy (referenced in Figure S6). We introduced a step in which we purified epidermal progenitor stem cells based on their preferential adherence to collagen IV (Murray et al., 1979; Bickenbach and Roop, 1999). In our hands, this step, which is a kind of physiological purification step that puts a minimal stress on the cells, resulted not only in a higher yield of hESC/iPSC-derived keratinocytes but also in a purified population that was highly homogeneous and similar to NHKs (Figure 2). Homogeneous

populations of keratinocytes differentiated from disease-specific iPSCs would be advantageous for addressing the effects of such mutations on keratinocyte biology (Mildner et al., 2010; Simpson et al., 2010).

Although a link between the level of ambient humidity and barrier development has been described in both animals (Hanley et al., 1997; Kömüves et al., 1999) and human premature infants (Agren et al., 2006), and then recapitulated in vitro with NHKs (Thakoersing et al., 2010), the exact molecular mechanism is still unclear. A limited number of studies have addressed the relationship between environmental humidity and barrier function in postnatal epidermis (Takei et al., 2013; Katagiri et al., 2003; Sato et al., 2002; Denda et al., 1998), and the results warrant further work. Regardless, the model that we describe here would have an unprecedented advantage for elucidating the molecular mechanisms of barrier development, perturbation, and recovery, as well as how mutations of genes involved in cornification and lipid metabolism affect permeability barrier homeostasis (Mildner et al., 2010; Simpson et al., 2010).

Previous HEE models have developed some barrier properties (Gschwandtner et al., 2013; Thakoersing et al., 2012; Ponec et al., 2001). The technique presented here is an advance from previously published HEEs because it is able to produce a HEE that not only shows morphologic changes associated with barrier establishment but also demonstrates the essential functional properties seen in skin with a functional barrier. The HEEs described above provide an effective block against water permeation, as evidenced by their ability to block lanthanum and form a calcium gradient. Further, this 3D model of HEEs with a functional permeability barrier is highly reproducible and has the potential to be easily scaled up and adapted to cGMP requirements for the use in regenerative and aesthetic medicine, as well as drug development. The recent (March 2013) European Union ban on the import and sale of cosmetics containing ingredients tested on animals will increase the demand for efficient and cost-effective alternative in vitro models that would not compromise consumer safety. HEEs with a functional permeability barrier generated completely in vitro from either hESCs or iPSCs, as described here, might present the best available answer (Küchler et al., 2013).

EXPERIMENTAL PROCEDURES

mRNA Synthesis and Modifications

The intronless coding sequences (CDSs) of *OCT4*, *SOX2*, *KLF4*, *c-MYC*, and *LIN28* were retrieved from the National Center for Biotechnology Information (NCBI). As previously described by Warren et al. (2010), a KOZAK translational initiation signal was added in the 5′ UTR, whereas the 3′ UTR was terminated with an alpha-globin-driven oligo(dT) sequence for templated addition of a polyA tail. The CDSs were then codon optimized with the use of GeneOptimizer expert software (GENEART/Life Technologies). Codon optimization allows more efficient transcription by avoiding RNA secondary structures, adjusting GC content, and removing splice-sites. The gene encoding the destabilized enhanced GFP (*d2EGFP*) codon from pRVGP-d2EGFP vector (Addgene) and optimized *OCT4*, *SOX2*, *KLF4*, *c-MYC*, and *LIN28* CDSs were synthesized and subcloned (GENEART/Life Technologies) into the pTNT plasmid vector, which was specifically designed for in vitro expression (Promega). Plasmids were linearized with BamHI. PCR templates were generated from the linearized plasmids using the same upstream primers for all six constructs and six different gene-specific, downstream T120-heeled reverse primers for addition of the poly(A) tail. Quality control of the PCR reaction was performed by capillary electrophoresis (Agilent Bioanalyzer). The templates were transcribed with T7 polymerase and further modified according to Warren et al. (2010). Modifications included the complete substitution of 5-methylcytidine (5mC) for cytidine and the substitution of pseudouridine (psi) for uridine to increase mRNA viability and ectopic protein expression. Furthermore, to promote efficient translation and increase mRNA half-life, a synthetic 5′ guanine cap 3′-0-Me-m7G(5′) ppp(5′)G was added and 5′-triphosphates were eliminated by Antarctic phosphatase treatment. The DNA template was removed with DNase, and single-strand RNA (ssRNA) was purified with spin columns. Quality control of the purified ssRNA product was performed by capillary electrophoresis (Agilent Bioanalyzer; Figure S1). An "mRNA cocktail" containing *OCT4*, *SOX2*, *KLF4*, *C-MYC*, *LIN28*, and d*2eGFP* in molar ratios of 3:1:1:1:1:1 at a final concentration of 100 ng/μl was prepared (AmsBio), aliquoted for single use, and frozen in single-use aliquots.

Reprogramming

Mitotically inactivated foreskin fibroblasts (NuFF from donor 11; AmsBio) were used as feeder cells and plated at a density of 2.5×10^5/well of a six-well dish coated with CELLstart (Life Technologies). Human neonatal foreskin fibroblasts BJ (ATCC, CRL-2522) were plated onto feeders 24 hr later at a density of 7,000/well. For each four wells to be transfected, 25 μl of RNAiMAX (Sigma), a lipofectamine transfection reagent, was diluted in 225 μl of Opti-MEM (Life Technologies) and mixed with 50 μl of mRNA cocktail diluted in 200 μl Opti-MEM. The complex was incubated at room temperature for 15 min before 120 ml was added dropwise into each of four wells to be transfected. The culture medium was refreshed 4 hr later with complete Pluriton medium (Stemgent) supplemented with 300 ng/ml B18R (eBioscience). Transfection was repeated for 17 consecutive days. On days 6–17, Pluriton was preconditioned with NuFF feeders for 24 hr and supplemented with 300 ng/ml B18R and 0.5 mM Na-butyrate. On days 18–21, potential iPSC colonies were left to expand in complete Pluriton with no other supplements. Ten colonies were picked based on morphology on day 21, transferred onto human foreskin fibroblast (HFF) feeders in KOSR-XF medium (Life Technologies), and expanded. Two clones with a similar growth rate, iKCL004 and iKCL011, were further characterized. The cells were cultured at 5% O_2, 37°C, 5% CO_2 throughout the reprogramming.

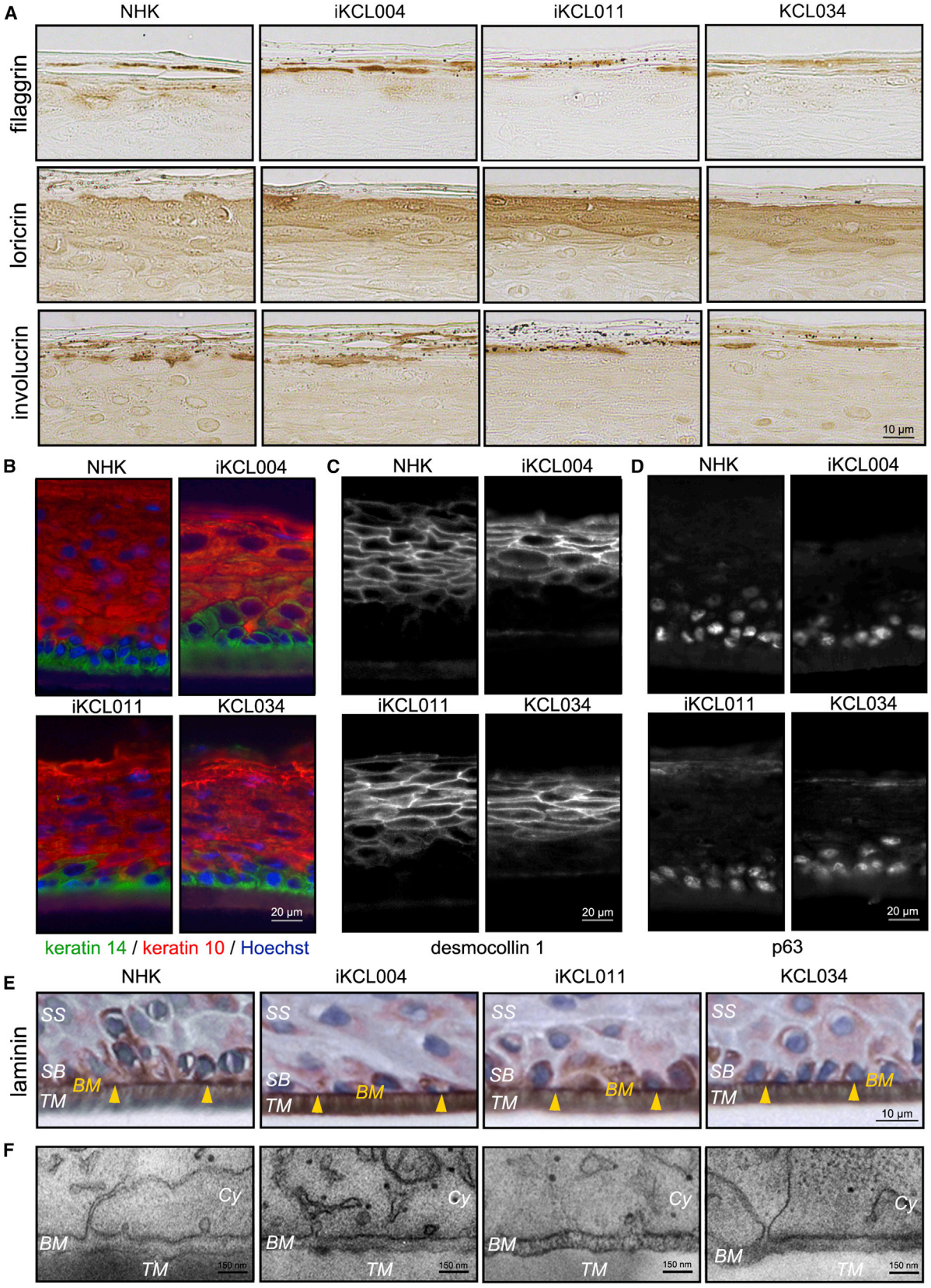

(legend on next page)

Characterization and Culture of PSCs

hESC line KCL034 was derived and characterized as previously described (Jacquet et al., 2013; Stephenson et al., 2012). Expression of pluripotency markers and capability to differentiate into cells of three germ layers were confirmed for both iKCL004 and iKCL011 by methods that are routinely used for hESC lines in our derivation center.

PSC lines were cultured under standard feeder-free conditions on BD Matrigel hESC-qualified matrix (Becton Dickinson) in mTESR1 medium (StemCell Technologies) under hypoxic (5% O_2) conditions.

Methylation Assay

Genomic DNA was isolated from BJ parental fibroblasts (negative control), KCL034 (positive control), iKCL004, and iKCL011. Each sample of 500 ng DNA was bisulfite treated (EZ Zymo DNA Kit) according to the manufacturer's recommendations optimized for 450k array. Epigenome-wide methylation (>480,000 CpG sites) was analyzed using the Infinium Human Methylation 450 BeadChip Kit (Illumina) in biological triplicates for each line. GenoSplice Technology performed quality control, processing, and further analyses of the data.

3D HDF ECM

Preparation of decellularized 3D ECM was performed as previously described (Ilic et al., 2012).

Differentiation Protocol

To induce differentiation, undifferentiated PSCs were transferred into a 20% O_2 atmosphere environment and treated with mTESR1 basal media supplemented with 1 μM ATRA (Sigma-Aldrich) and 25 ng/ml BMP4 (R&D) for 7 days (*Induction*). To select for cells with early acquisition of ectodermal fate, the cells were harvested and replated onto freshly prepared 3D HDF ECM at a density of 5–10 × 10^3 cells per cm^2 and grown in Dulbecco's modified Eagle's medium/Ham F12 (3:1; Life Technologies) supplemented with 1 μM ATRA and 25 ng/ml BMP4 for a further 7 days (*Selection*). To enrich for putative epidermal progenitors, rapid adhesion to type IV collagen-coated dishes was used, and the rapidly adhering cells were cultured in defined keratinocyte-SFM supplemented with 1 μM ATRA for 7 days (*Enrichment*). After that, the cells were cultured in EpiLife medium (Life Technologies) for a further 7 days (*Expansion*) before final harvest and analysis.

Proliferation Assay

All three lines and NHKs were seeded in six-well plates in triplicates at a constant density of 4 × 10^5 per well. Every 7 days, cells were harvested and the total number was counted. The cells were then subcultured at the density described above. This cycle was repeated for five passages. Average PDs were calculated for each line and control at each passage according to the following formula:

PD = (log 2) − 1(logNt − logN0), where Nt = cell number at harvest and N0 = cell number plated (4 × 10^5). The total PD level was calculated as the cumulative of average PDs for five passages. The PDT was calculated according to the following formula: PDT = I/PD, where I = interval (days) between the passages (7).

Immunostaining

Samples were processed as previously described (Ilic et al., 2007; Stephenson et al., 2012). The following antibodies were used: rabbit anti-K14, rabbit anti-filaggrin, rabbit anti-involucrin, and rabbit anti-loricrin (all from Covance); rabbit anti-laminin (DAKO); mouse anti-p63 (Santa Cruz Biotechnology); rabbit anti-fibronectin, mouse anti-collagen IV, mouse anti-collagen VII, and rabbit anti-desmocollin 1 (all from Sigma-Aldrich); and rabbit anti-p63, mouse anti-K10, and rabbit anti-collagen I (all from Abcam). Secondary antibodies were obtained from Jackson ImmunoResearch and Life Technologies.

Flow Cytometry with Confocal Imaging

Cells were incubated with PE-conjugated rat anti-CD104 (integrin β4) antibody (BD PharMingen) for 1 hr, washed, fixed with 4% (v/v) paraformaldehyde, and permeabilized with 0.1% Triton X-100 in PBS. The samples were then incubated with fluorescein isothiocyanate (FITC)-conjugated mouse anti-K14 antibody (Abcam) for 1 hr, washed and incubated with Hoescht 33342 (Life Technologies) for 5 min. To set the gating, fluorescence minus one (FMO) and single-stained compensation controls were also prepared. For acquisition, 1 × 10^6 cells/per sample were resuspended in 100 μl of 1% BSA/PBS. The data were acquired on an ImageStream^X analyzer and analyzed with IDEAS software (Amnis).

Quantitative RT-PCR

Data for quantitative PCR (qPCR) analysis were collected from three independently performed differentiation rounds for each of the cell lines. Total RNA extraction was performed at T0, T1, T2, and T3 time points using the RNeasy kit (QIAGEN). For cDNA preparation, the QuantiTect Reverse Transcription Kit (-QIAGEN) was used. The primers are listed in Figure S7. KAPA SYBR FAST Universal 2× qPCR Master Mix (Kapa Biosystems) was used to set up the qPCR and run on a real-time PCR 7900HT system (Applied Biosystems). All reactions were run in triplicates. The data were collected and analyzed using GUSB and β-actin

Figure 6. The Distribution of Epidermal Markers in HEEs Mirrors that in Human Skin

(A) Immunostaining for three markers of keratinocyte terminal differentiation: filaggrin, loricrin, and involucrin. Each of these markers is expressed at the appropriate site, denoting normal epidermal differentiation.

(B–D) Immunostaining for K14 (basal layer) and K10 (suprabasal layers) (B), desmocollin 1 (suprabasal layers) (C), and p63 (basal layer in general) (D) demonstrates normal epithelial stratification in all HEE cultures.

(E and F) Basal layer keratinocytes express laminin (E) and form BMZ-like structure (F). BM, basement membrane; Cy, cytoplasm; SB, stratum basale; TM, transwell membrane. Yellow arrowheads point to laminin-positive staining of BM.

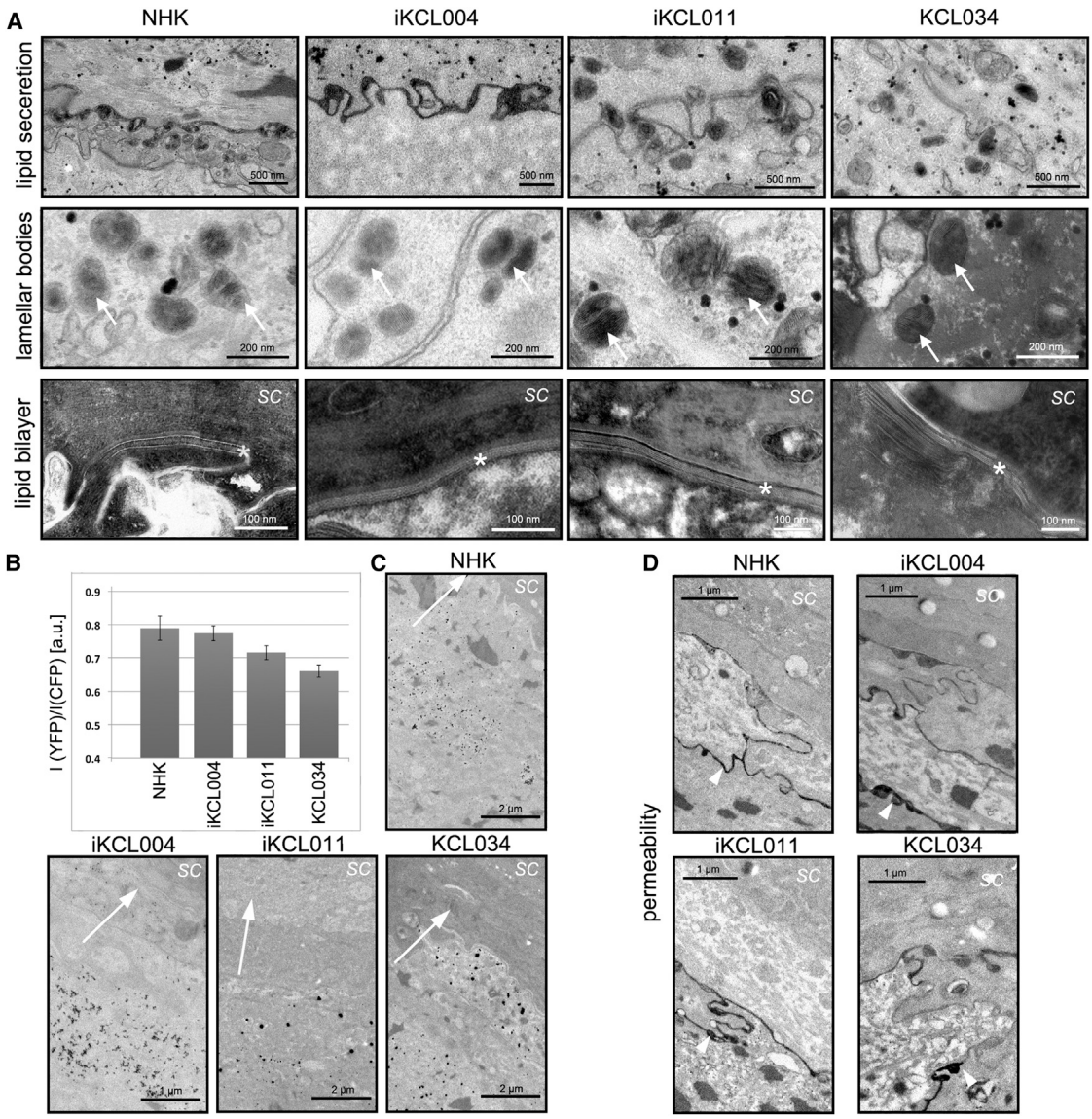

Figure 7. HEE with a Functional Permeability Barrier

(A) Lipid bilayer formation assessed with TEM. Arrows, lamellar bodies; asterisks, lipid bilayers. Upper row: normal lipid secretion between the SG and SC is seen in all cultures. Middle row: LBs are seen in the SG of all cultures (arrows). LB morphology was normal in all cultures, although it appeared slightly smudged in KCL034. Bottom row: lipid was successfully processed into lipid bilayers (asterisks) in all cultures. Like LB morphology, lipid bilayer morphology was normal in all cultures, although it seems slightly disrupted in KCL034.

(B) ER Ca^{2+} sequestration at day 7 of HEE culture in cells transfected with the ER-targeted Ca^{2+} sensor D1ER. Data are presented as the mean of the intensity ratio (I) between the yellow-channel (higher Ca^{2+}) and blue-channel (lower Ca^{2+}) images (I(yfp)/I(cfp)) ± SEM. Higher ratios denote higher Ca^{2+} stores in the ER. n = 10–14 cells from two biological replicates in each group. Significance was calculated using a one-way ANOVA. Distributions with $p < 0.05$ were assumed to be statistically different based on unpaired t tests between the populations.

(C) The epidermal Ca^{2+} gradient captured on TEM as electron-dense Ca^{2+} deposits at day 14. Arrows indicate the direction from the basal layer toward the SC. Ca^{2+} precipitates (black deposits) denote the presence of Ca^{2+} in the tissue. Precipitates are seen in the viable SG but are absent from the SC, denoting a functional barrier to the passage of water and ions.

(D) Permeability barrier integrity assessed by lanthanum perfusion. Lanthanum is visualized as electron-dense deposits in the extracellular spaces of the viable SG (arrowheads), demonstrating that lanthanum and, by extension, water and other small ions can pass between keratinocytes in this stratum. In contrast, lanthanum spreads along the base of the SC, but cannot penetrate further into the SC because a functioning lipid barrier is blocking its movement upward. All cultures demonstrated a functional permeability barrier.

or GAPDH as the reference genes. The results were analyzed and quantified using the ddCT method.

Whole-Genome Gene-Expression Array

Total RNA from T3 cell populations and control primary NHKs were reverse transcribed into cDNA using SuperScript III Reverse Transcriptase (Life Technologies). In vitro transcription of biotin-labeled antisense RNA (aRNA) was performed with the TargetAmp-Nano labeling kit (Epicenter), and purification was performed with the RNeasy Mini Kit (QIAGEN). The quality and quantity of the resultant biotin-labeled aRNAs were assessed using a Bioanalyzer (Agilent) and Qubit Fluorometer (Life Technologies). A total amount of 750 ng of biotin-labeled aRNA in a 5 μl volume was then used for the HumanHT-12 Expression BeadChip whole-genome, gene-expression direct hybridization assay system (Illumina) according to the manufacturer's instructions and run on the iScan system (Illumina).

HEEs

A suspension of 0.25 × 10^6 neonatal NHKs or hESC/iPSC-derived keratinocytes was seeded on a CELLstart CTS (Invitrogen)-coated 12-well 0.4 μm PET Millicell Hanging Cell Culture Insert (Millipore) in CnT.BM.1 medium with CnT-07 supplement (CELLnTEC). Three days after seeding, the medium was switched to CnT-BM.3 medium with CnT-02-3DF with supplement (CELLnTEC). On day 4, the HEEs were air exposed by feeding the insert from bottom of the well only. HEEs were grown in a humidified (×100% relative humidity) or dry (30%–50% relative humidity) incubator at 37°C (R.S., A.C., D.C., M.H., L.C., S.D. Peckenpacker, K. Park, Y. Uchida, K.R. Feingold, P.M. Elias, D.I., and T.M.M., unpublished data). The TEER was measured with an epithelial voltohmmeter (EVOM; World Precision Instruments).

ER Ca^{2+} Sequestration

Cells were transfected with the ER-targeted cameleon-based Ca^{2+} sensor D1ER (a gift from Dr. Amy Palmer; Palmer and Tsien, 2006) using the lipid-based *Trans*IT transfection reagent (Mirus) at a 1:3 DNA/*Trans*IT ratio. Transfection complexes were assembled 30 min prior to cell plating by adding 1 μl D1ER (at a 1.3 μg/μl concentration) and 3 μl transfection reagent per 100 μl serum-free OptiMem. Cells were resuspended in low-calcium 154 CF medium supplemented with 0.03 mM Ca^{2+} (GIBCO) at a density of 0.5 × 10^6 cells per 1.5 ml. Transfection complexes were added to the suspension at a 100 μl:1 ml complex/cell suspension ratio and gently mixed by pipetting. The cells were then plated into 12-well inserts precoated with CELLstart at a 0.5 × 10^6 cells per insert density and left with the transfection complexes overnight. The medium was then switched to CnT.BM.1 medium with CnT-07 supplement (CELLnTEC) for 3 days. Dual-channel fluorescence measurements were recorded using a Zeiss LSM Meta confocal system (Zeiss).

Transmission Electron Microscopy

Samples were processed for transmission electron microscopy (TEM) as previously described (Ilic et al., 2007; Tu et al., 2012).

ACCESSION NUMBERS

The methylation data have been deposited in the Gene Expression Omnibus under accession number GSE55006, and expression array data have been deposited under accession number GSE55898.

SUPPLEMENTAL INFORMATION

Supplemental Information includes seven figures and seven tables and can be found with this article online at http://dx.doi.org/10.1016/j.stemcr.2014.03.009.

ACKNOWLEDGMENTS

For help and support, we thank H. Navsaria and G. Damodaran (Cell and Tissue Engineering, Centre for Cutaneous Research, Queen Mary, University of London), W.-L. Di (Institute of Child Health, University College London), S. Minger (GE Healthcare), and the staffs of the San Francisco Veteran Affairs Medical Center, the Genomics and Flow Cytometry facilities, and the Biomedical Research Centre at Guy's Hospital. We also thank C. Ogilvie from the Genetics Centre at Guy's Hospital for a critical reading of the manuscript. This work was supported in part by grants from the Medical Research Council UK (G0801061 to D.I.), the NIH (R21 ARO61583 and R01 AR051930), the Research Service of the Department of Veterans Affairs (to T.M.M.), and the Dystrophic Epidermolysis Bullosa Research Association (DebRA) (to J.A.M.). A.P. was a DebRA-supported PhD student.

Received: November 19, 2013
Revised: March 25, 2014
Accepted: March 26, 2014
Published: April 24, 2014

REFERENCES

Aberdam, D., Gambaro, K., Rostagno, P., Aberdam, E., de la Forest Divonne, S., and Rouleau, M. (2007). Key role of p63 in BMP-4-induced epidermal commitment of embryonic stem cells. Cell Cycle *6*, 291–294.

Agren, J., Sjörs, G., and Sedin, G. (2006). Ambient humidity influences the rate of skin barrier maturation in extremely preterm infants. J. Pediatr. *148*, 613–617.

Bellin, M., Marchetto, M.C., Gage, F.H., and Mummery, C.L. (2012). Induced pluripotent stem cells: the new patient? Nat. Rev. Mol. Cell Biol. *13*, 713–726.

Bickenbach, J.R., and Roop, D.R. (1999). Transduction of a preselected population of human epidermal stem cells: consequences for gene therapy. Proc. Assoc. Am. Physicians *111*, 184–189.

Blanpain, C., and Fuchs, E. (2007). p63: revving up epithelial stem-cell potential. Nat. Cell Biol. *9*, 731–733.

Blanpain, C., and Fuchs, E. (2009). Epidermal homeostasis: a balancing act of stem cells in the skin. Nat. Rev. Mol. Cell Biol. *10*, 207–217.

Callewaert, G., Parys, J.B., De Smedt, H., Raeymaekers, L., Wuytack, F., Vanoevelen, J., Van Baelen, K., Simoni, A., Rizzuto, R., and Missiaen, L. (2003). Similar $Ca^{(2+)}$-signaling properties in keratinocytes and

in COS-1 cells overexpressing the secretory-pathway Ca(2+)-ATPase SPCA1. Cell Calcium *34*, 157–162.

Celli, A., Mackenzie, D.S., Zhai, Y., Tu, C.-L., Bikle, D.D., Holleran, W.M., Uchida, Y., and Mauro, T.M. (2012). SERCA2-controlled Ca^2+-dependent keratinocyte adhesion and differentiation is mediated via the sphingolipid pathway: a therapeutic target for Darier's disease. J. Invest. Dermatol. *132*, 1188–1195.

Chang, C., and Hemmati-Brivanlou, A. (1998). Cell fate determination in embryonic ectoderm. J. Neurobiol. *36*, 128–151.

Cheng, X., Ying, L., Lu, L., Galvão, A.M., Mills, J.A., Lin, H.C., Kotton, D.N., Shen, S.S., Nostro, M.C., Choi, J.K., et al. (2012). Self-renewing endodermal progenitor lines generated from human pluripotent stem cells. Cell Stem Cell *10*, 371–384.

Crum, C.P., and McKeon, F.D. (2010). p63 in epithelial survival, germ cell surveillance, and neoplasia. Annu. Rev. Pathol. *5*, 349–371.

Del Rio, M., Larcher, F., Serrano, F., Meana, A., Muñoz, M., Garcia, M., Muñoz, E., Martin, C., Bernad, A., and Jorcano, J.L. (2002). A preclinical model for the analysis of genetically modified human skin in vivo. Hum. Gene Ther. *13*, 959–968.

Denda, M., Sato, J., Masuda, Y., Tsuchiya, T., Koyama, J., Kuramoto, M., Elias, P.M., and Feingold, K.R. (1998). Exposure to a dry environment enhances epidermal permeability barrier function. J. Invest. Dermatol. *111*, 858–863.

Elias, P.M. (1983). Epidermal lipids, barrier function, and desquamation. J. Invest. Dermatol. Suppl. *80*, 44s–49s.

Elias, P.M. (2012). Structure and function of the stratum corneum extracellular matrix. J. Invest. Dermatol. *132*, 2131–2133.

Elias, P.M., Ahn, S.K., Denda, M., Brown, B.E., Crumrine, D., Kimutai, L.K., Kömüves, L., Lee, S.H., and Feingold, K.R. (2002). Modulations in epidermal calcium regulate the expression of differentiation-specific markers. J. Invest. Dermatol. *119*, 1128–1136.

Götz, C., Pfeiffer, R., Tigges, J., Blatz, V., Jäckh, C., Freytag, E.M., Fabian, E., Landsiedel, R., Merk, H.F., Krutmann, J., et al. (2012). Xenobiotic metabolism capacities of human skin in comparison with a 3D epidermis model and keratinocyte-based cell culture as in vitro alternatives for chemical testing: activating enzymes (Phase I). Exp. Dermatol. *21*, 358–363.

Gschwandtner, M., Mildner, M., Mlitz, V., Gruber, F., Eckhart, L., Werfel, T., Gutzmer, R., Elias, P.M., and Tschachler, E. (2013). Histamine suppresses epidermal keratinocyte differentiation and impairs skin barrier function in a human skin model. Allergy *68*, 37–47.

Hanley, K., Jiang, Y., Elias, P.M., Feingold, K.R., and Williams, M.L. (1997). Acceleration of barrier ontogenesis in vitro through air exposure. Pediatr. Res. *41*, 293–299.

Hay, D.C., Zhao, D., Fletcher, J., Hewitt, Z.A., McLean, D., Urruticoechea-Uriguen, A., Black, J.R., Elcombe, C., Ross, J.A., Wolf, R., and Cui, W. (2008). Efficient differentiation of hepatocytes from human embryonic stem cells exhibiting markers recapitulating liver development in vivo. Stem Cells *26*, 894–902.

Ilic, D., Mao-Qiang, M., Crumrine, D., Dolganov, G., Larocque, N., Xu, P., Demerjian, M., Brown, B.E., Lim, S.T., Ossovskaya, V., et al. (2007). Focal adhesion kinase controls pH-dependent epidermal barrier homeostasis by regulating actin-directed Na^+/H^+ exchanger 1 plasma membrane localization. Am. J. Pathol. *170*, 2055–2067.

Ilic, D., Stephenson, E., Wood, V., Jacquet, L., Stevenson, D., Petrova, A., Kadeva, N., Codognotto, S., Patel, H., Semple, M., et al. (2012). Derivation and feeder-free propagation of human embryonic stem cells under xeno-free conditions. Cytotherapy *14*, 122–128.

Itoh, M., Umegaki-Arao, N., Guo, Z., Liu, L., Higgins, C.A., and Christiano, A.M. (2013). Generation of 3D skin equivalents fully reconstituted from human induced pluripotent stem cells (iPSCs). PLoS ONE *8*, e77673.

Jacquet, L., Stephenson, E., Collins, R., Patel, H., Trussler, J., Al-Bedaery, R., Renwick, P., Ogilvie, C., Vaughan, R., and Ilic, D. (2013). Strategy for the creation of clinical grade hESC line banks that HLA-match a target population. EMBO Mol Med *5*, 10–17.

Kalinin, A.E., Kajava, A.V., and Steinert, P.M. (2002). Epithelial barrier function: assembly and structural features of the cornified cell envelope. Bioessays *24*, 789–800.

Katagiri, C., Sato, J., Nomura, J., and Denda, M. (2003). Changes in environmental humidity affect the water-holding property of the stratum corneum and its free amino acid content, and the expression of filaggrin in the epidermis of hairless mice. J. Dermatol. Sci. *31*, 29–35.

Kömüves, L.G., Hanley, K., Jiang, Y., Katagiri, C., Elias, P.M., Williams, M.L., and Feingold, K.R. (1999). Induction of selected lipid metabolic enzymes and differentiation-linked structural proteins by air exposure in fetal rat skin explants. J. Invest. Dermatol. *112*, 303–309.

Küchler, S., Strüver, K., and Friess, W. (2013). Reconstructed skin models as emerging tools for drug absorption studies. Expert Opin. Drug Metab. Toxicol. *9*, 1255–1263.

Linde, N., Gutschalk, C.M., Hoffmann, C., Yilmaz, D., and Mueller, M.M. (2012). Integrating macrophages into organotypic co-cultures: a 3D in vitro model to study tumor-associated macrophages. PLoS ONE *7*, e40058.

Medawar, A., Virolle, T., Rostagno, P., de la Forest-Divonne, S., Gambaro, K., Rouleau, M., and Aberdam, D. (2008). DeltaNp63 is essential for epidermal commitment of embryonic stem cells. PLoS ONE *3*, e3441.

Mildner, M., Jin, J., Eckhart, L., Kezic, S., Gruber, F., Barresi, C., Stremnitzer, C., Buchberger, M., Mlitz, V., Ballaun, C., et al. (2010). Knockdown of filaggrin impairs diffusion barrier function and increases UV sensitivity in a human skin model. J. Invest. Dermatol. *130*, 2286–2294.

Murray, J.C., Stingl, G., Kleinman, H.K., Martin, G.R., and Katz, S.I. (1979). Epidermal cells adhere preferentially to type IV (basement membrane) collagen. J. Cell Biol. *80*, 197–202.

Nemes, Z., and Steinert, P.M. (1999). Bricks and mortar of the epidermal barrier. Exp. Mol. Med. *31*, 5–19.

Nissan, X., Larribere, L., Saidani, M., Hurbain, I., Delevoye, C., Feteira, J., Lemaitre, G., Peschanski, M., and Baldeschi, C. (2011). Functional melanocytes derived from human pluripotent stem cells engraft into pluristratified epidermis. Proc. Natl. Acad. Sci. USA *108*, 14861–14866.

Palmer, A.E., and Tsien, R.Y. (2006). Measuring calcium signaling using genetically targetable fluorescent indicators. Nat. Protoc. *1*, 1057–1065.

Ponec, M., Gibbs, S., Pilgram, G., Boelsma, E., Koerten, H., Bouwstra, J., and Mommaas, M. (2001). Barrier function in reconstructed epidermis and its resemblance to native human skin. Skin Pharmacol. Appl. Skin Physiol. *14* (*Suppl 1*), 63–71.

Pozzi, S., Zambelli, F., Merico, D., Pavesi, G., Robert, A., Maltère, P., Gidrol, X., Mantovani, R., and Vigano, M.A. (2009). Transcriptional network of p63 in human keratinocytes. PLoS ONE *4*, e5008.

Richard, G. (2004). Molecular genetics of the ichthyoses. Am. J. Med. Genet. C. Semin. Med. Genet. *131C*, 32–44.

Robinton, D.A., and Daley, G.Q. (2012). The promise of induced pluripotent stem cells in research and therapy. Nature *481*, 295–305.

Sato, J., Denda, M., Chang, S., Elias, P.M., and Feingold, K.R. (2002). Abrupt decreases in environmental humidity induce abnormalities in permeability barrier homeostasis. J. Invest. Dermatol. *119*, 900–904.

Segre, J. (2003). Complex redundancy to build a simple epidermal permeability barrier. Curr. Opin. Cell Biol. *15*, 776–782.

Segre, J.A. (2006). Epidermal barrier formation and recovery in skin disorders. J. Clin. Invest. *116*, 1150–1158.

Simpson, C.L., Kojima, S., and Getsios, S. (2010). RNA interference in keratinocytes and an organotypic model of human epidermis. Methods Mol. Biol. *585*, 127–146.

Simpson, C.L., Patel, D.M., and Green, K.J. (2011). Deconstructing the skin: cytoarchitectural determinants of epidermal morphogenesis. Nat. Rev. Mol. Cell Biol. *12*, 565–580.

Smith, F.J., Irvine, A.D., Terron-Kwiatkowski, A., Sandilands, A., Campbell, L.E., Zhao, Y., Liao, H., Evans, A.T., Goudie, D.R., Lewis-Jones, S., et al. (2006). Loss-of-function mutations in the gene encoding filaggrin cause ichthyosis vulgaris. Nat. Genet. *38*, 337–342.

Stephenson, E., Jacquet, L., Miere, C., Wood, V., Kadeva, N., Cornwell, G., Codognotto, S., Dajani, Y., Braude, P., and Ilic, D. (2012). Derivation and propagation of human embryonic stem cell lines from frozen embryos in an animal product-free environment. Nat. Protoc. *7*, 1366–1381.

Stern, C.D. (2005). Neural induction: old problem, new findings, yet more questions. Development *132*, 2007–2021.

Takei, K., Denda, S., Kumamoto, J., and Denda, M. (2013). Low environmental humidity induces synthesis and release of cortisol in an epidermal organotypic culture system. Exp. Dermatol. *22*, 662–664.

Thakoersing, V.S., Ponec, M., and Bouwstra, J.A. (2010). Generation of human skin equivalents under submerged conditions-mimicking the in utero environment. Tissue Eng. Part A *16*, 1433–1441.

Thakoersing, V.S., Gooris, G.S., Mulder, A., Rietveld, M., El Ghalbzouri, A., and Bouwstra, J.A. (2012). Unraveling barrier properties of three different in-house human skin equivalents. Tissue Eng. Part C Methods *18*, 1–11.

Tu, C.-L., Crumrine, D.A., Man, M.-Q., Chang, W., Elalieh, H., You, M., Elias, P.M., and Bikle, D.D. (2012). Ablation of the calcium-sensing receptor in keratinocytes impairs epidermal differentiation and barrier function. J. Invest. Dermatol. *132*, 2350–2359.

Vanbokhoven, H., Melino, G., Candi, E., and Declercq, W. (2011). p63, a story of mice and men. J. Invest. Dermatol. *131*, 1196–1207.

Warren, L., Manos, P.D., Ahfeldt, T., Loh, Y.H., Li, H., Lau, F., Ebina, W., Mandal, P.K., Smith, Z.D., Meissner, A., et al. (2010). Highly efficient reprogramming to pluripotency and directed differentiation of human cells with synthetic modified mRNA. Cell Stem Cell *7*, 618–630.

Yakubov, E., Rechavi, G., Rozenblatt, S., and Givol, D. (2010). Reprogramming of human fibroblasts to pluripotent stem cells using mRNA of four transcription factors. Biochem. Biophys. Res. Commun. *394*, 189–193.